JOURNAL OF APPLIED PHYSICS **105**, 094505 (2009)

The impact of barrier height distributions in tunnel junctions

Casey W. Miller[a)] and Dustin D. Belyea
Department of Physics, Center for Integrated Functional Materials, University of South Florida, 4202 East Fowler Avenue, Tampa, Florida 33620, USA

(Received 19 February 2009; accepted 25 March 2009; published online 12 May 2009)

We demonstrate that including continuous and discrete tunnel barrier height distributions in otherwise traditional tunneling formalisms enables straightforward modeling of several phenomena important to tunneling. Random barrier height inhomogeneities significantly impact the tunneling conductance, as evidenced by ideal tunneling models extracting faulty barrier parameters, with the incurred errors strongly dependent on the variance. Thermal smearing is addressed by transferring the energy distribution from the electrons to the barrier potential energy, thereby enabling zero-temperature tunneling models to model temperature dependent tunneling. For discrete tunneling channels, a secondary, impuritylike channel is shown to dominate the net conductance at surprisingly low impurity levels, implying that the observation of intrinsically large barrier heights is highly unlikely with transport measurements. Finally, spin-filter tunneling is modeled with independent tunneling channels whose barrier heights are linked to a temperature-dependent exchange splitting. [DOI: 10.1063/1.3122600]

I. INTRODUCTION

The bias dependence of the tunneling conductance of metal-insulator-metal (MIM) tunnel junctions are generally fit to Wentzel–Kramers–Brillouin (WKB)-based models, such as those of Brinkman, Dynes, and Rowell (BDR) (Ref. 1) or Simmons,[2] using the thickness (s) and interfacial barrier heights (ϕ_1 and ϕ_2) as adjustable parameters. These models compare the performance of a device to an ideal junction at $T=0$ K, where the barrier thickness and two interfacial heights are uniform throughout the junction. In reality, all tunneling devices have a distribution of barrier thicknesses and heights. Miller *et al.*[3] recently demonstrated that experimentally validated amounts of interfacial roughness[4,5] cannot only cause errors in the extracted barrier parameters, but can also cause the tunneling conductance to remain parabolic out to anomalously high biases;[6] a similar bias dependence was observed in superconducting junctions.[7] The existence of barrier height distributions in real devices has been demonstrated by ballistic electron emission microscopy[8,9] and scanning tunneling spectroscopy (on half-formed MgO junctions).[10] Other measurements investigating the barrier heights, including standard transport measurements and photoconductance,[11] simultaneously sample large fractions of the junction area, and are thus not conducive to the direct determination of a distribution of barrier heights.

In this work we investigate the impact of nonuniform barrier height distributions on MIM tunnel junctions. We develop a method for simulating the net tunneling conductance of a junction that has an arbitrarily defined distribution of barrier heights. Continuous and discrete barrier height distributions are considered. The former is illustrated in the context of a random distribution of heights, and is used to enable the temperature dependence of a junction to be simulated with zero temperature models. The latter is illustrated with two-channel conduction, including a demonstration of spin-filter tunneling.

II. SIMULATION DETAILS

We calculate the tunneling current density using an expansion of the model of BDR (Ref. 1) as

$$j = G_o\left(V + \frac{s\sqrt{2m/q}\Delta\phi}{24\hbar\bar{\phi}^{3/2}}V^2 + \frac{s^2mq}{12\hbar^2\bar{\phi}}V^3\right), \qquad (1)$$

where the leading term is the tunneling conductance at zero bias,

$$G_o = \left(\frac{q}{h}\right)^2\left(\frac{2mq\bar{\phi}}{s^2}\right)^{1/2}\exp\left(-\frac{2s}{\hbar}\sqrt{2mq\bar{\phi}}\right).$$

Here, s (in meters) is the barrier thickness, $\bar{\phi}$ (in Volts) is the position- and bias-dependent average barrier height, $\Delta\phi$ is the interfacial barrier height difference at zero bias (in Volts), q (in Coulombs) is the elementary charge, and m (in kilogram) is the electron mass. This expansion is only valid for biases less than one-third of the barrier height,[6] above which higher order terms take over as the system tends toward the Fowler–Nordheim tunneling regime. In what follows, we calculated the net current density via Eq. (1) for arbitrary distributions of individual barrier heights ϕ_n by weighting each corresponding current density $j(\phi_n)$ with a ϕ-dependent coefficient $\alpha(\phi_n)$, then summing these as parallel conduction channels: $j_{\text{net}}=\Sigma_n\alpha(\phi_n)j(\phi_n,s,V)$. Regardless of its specific form, the normalized coefficients represent the relative area of the junction with height ϕ_n.[12] A height step size ($\delta\phi=\phi_i-\phi_{i-1}$) of 0.5 meV was used because the results were independent of $\delta\phi$ less than this value. This formalism is general for asymmetric barriers, but we assume symmetric barriers at zero bias for computational ease (i.e., $\alpha(\phi_n)$ is used for both interfacial barrier heights). The net conductance was fit with

[a)]Electronic mail: cmilleratphysics@gmail.com.

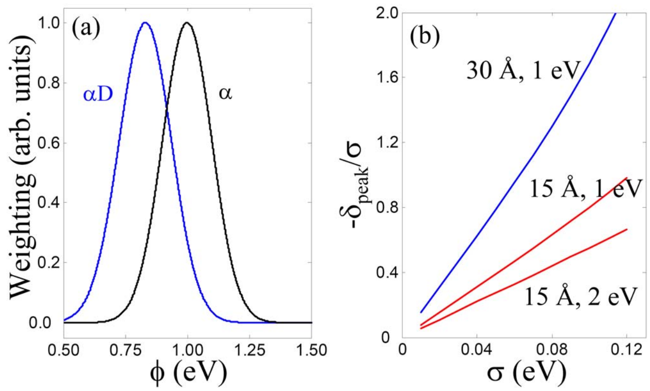

FIG. 1. (Color online) (a) Normalized Gaussian weighting coefficients $\alpha(\phi_n)$ (black) for $\phi_n=1.0\pm0.1$ eV, and related $\alpha\times$D (blue), which is the relative contribution of each height to G_{net} (D is the tunneling probability). (b) The peak of $\alpha\times$D shifts from the peak barrier height by an amount δ_{peak}, which can be a significant fraction of the standard deviation of the height distribution. The peak corresponds to the channel dominating the conductance.

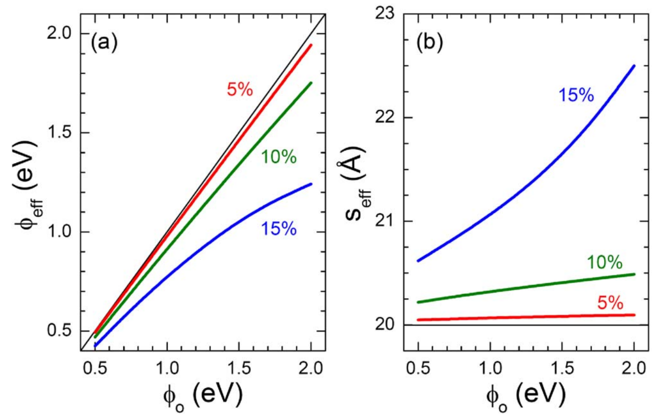

FIG. 2. (Color online) Effective barrier height (a) and width (b) determined by fits of G_{net} vs V for $s=20$ Å as functions of ϕ_o and σ (as noted in percent of ϕ_o). Thin black lines indicate $\phi_{eff}=\phi_o$ or $s_{eff}=s_o$.

the ideal BDR model to determine the effective barrier height and width; fits were performed using an appropriate bias range.[6]

III. CONTINUOUS DISTRIBUTIONS

A. Gaussian distribution

As a first approximation to randomness in the barrier height, we assume a properly normalized Gaussian distribution of weighting coefficients: $\alpha(\phi_n)/\Sigma_n\alpha(\phi_n)$, where $\alpha(\phi_n)=\exp[-(\phi_n-\phi_o)^2/(2\sigma^2)]$. These weighting coefficients and their product with the tunneling probability, $D(s,\phi)$, are shown in Fig. 1(a) for $\phi_o=1$ eV, $\sigma=0.1$ eV, and $s=15$ Å. $D(s,\phi)=\exp\left(-\frac{2}{\hbar}\int_0^s\sqrt{2m\phi(x,V,E)}dx\right)$ is the exponential term in the full tunneling integral,[1] and $\alpha\times D$ is thus the integrand of that equation (neglecting the Fermi functions). The mean of the $\alpha\times D$ distribution is thus the barrier height that contributes the most to the net tunneling current density. Figure 1(b) shows that the shift of the $\alpha\times D$ peak is most significant for thick, low barriers. In this example, the shift approaches 2σ for a 30 Å, 1 eV barrier with $\sigma\sim0.1$ eV. Thus, these data show that an experimentally reasonable[13,14] standard deviation of 10% results in sparse regions of the sample, with barrier heights lower than the mean height, heavily influencing the net conductance. These are known colloquially as "hot spots" and can also originate from junctions with uniform barrier heights and thickness distributions.[3] In reality of course, a junction will have both barrier height and thickness distributions, which are probably strongly correlated because the electronic structure of many materials is strongly thickness-dependent on the length scales of tunneling (a few lattice constants).

The net conductance calculated including barrier height distributions closely resembles that of single-height barriers. Thus, modeling these data under the faulty assumption of a unique barrier height would produce a statistically good fit, although the resulting effective barrier parameters may be erroneous. Figure 2 illustrates this by showing the best fit parameters, ϕ_{eff} and s_{eff}, as functions of ϕ_o and σ with $s=20$ Å when the net conductance is fit with the BDR model (which assumes $\sigma\equiv0$). From this single-height perspective, increasing σ causes a reduced effective height and an increased effective barrier thickness. The impact of the height distribution on the effective height is qualitatively similar to what was observed for the impact of surface roughness on effective thickness.[3]

B. Thermal smearing

Thermal smearing is an important aspect of tunneling that can also be addressed with a continuous barrier height distribution. The impact of thermal smearing has been known for some time in superconductor-based junctions,[15,16] but only recently pointed out for magnetic tunnel junctions.[17–19] Thermal smearing is present in all tunneling measurements, even if other thermal effects exist simultaneously (e.g., temperature-dependent spin polarization of electrodes in magnetic tunnel junctions[20]). According to Rowell's tunneling criteria,[16] the temperature dependence of a tunnel junction should be due solely to thermal smearing. In fact, this is the only of Rowell's criteria that both survives for normal-state junctions[21,22] and can be used to conclusively comment on the existence of pinhole shorts.[23,24]

The treatment of thermal smearing is usually left to the Fermi terms in the full tunneling integral.[1] This works perfectly well for calculations, but is difficult to include when fitting data with established tunneling formalisms that tacitly assume zero temperature, such as the omnipresent BDR and Simmons models. The method we present is a bridge to allow temperature dependences to be included within these simple, yet powerful models.

At finite temperature, thermal excitations cause the electrons within the electrodes to have a distribution of energies with mean energy E_f, as indicated by the color gradient in Fig. 3(a). The distribution is proportional to $|df/dE|$ versus E, is symmetric about the Fermi Energy (E_f), and has a full width at half maximum (FWHM) equal to 3.53 k_BT. All electrons are able to tunnel, but they each see a different, energy-dependent tunnel barrier height. Hot electrons with energy $E_f+\delta_E$ see a lower barrier height $\phi_{hot}=\phi_o-\delta_E$, while cold electrons see a higher height $\phi_{cold}=\phi_o+\delta_E$. Because the

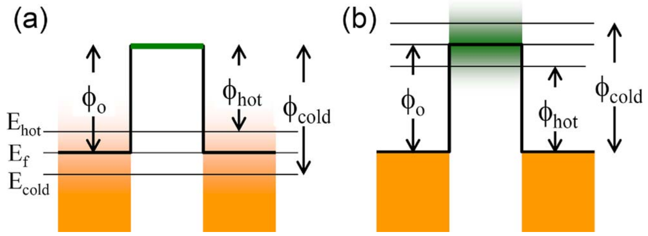

FIG. 3. (Color online) Equivalence of thermal smearing and a barrier height distribution. The smearing of the Fermi distribution in electrodes at finite temperature, as in (a), implies that hot (cold) electrons see a lower (higher) barrier height. Finite temperature can thus be modeled using zero temperature electrodes and a distribution of barrier heights, as in (b), where the distribution is derived from the Fermi function.

tunneling probability is proportional to $\exp(-\sqrt{\phi})$, hot electrons dominate the tunneling process. If we make a temperature-dependent transformation so that each electron has energy E_f, then the tunnel barrier acquires a distribution of heights, as indicated by the color gradient in Fig. 3(b). This is simply a deconvolution of the entire energy diagram, including the zero-temperature barrier potential energy, with a function appropriate to produce a zero-temperature Fermi distribution in the electrodes. Then, using the basic formalism noted above, we may evaluate the temperature dependence of the junction by adjusting kT in the Fermi–Dirac barrier height distribution. Thus, we assume a properly normalized distribution of weighting coefficients, $\alpha(\phi_n)/\Sigma_n\alpha(\phi_n)$, where

$$\alpha(\phi_n) = \left| \frac{d}{dE}\frac{1}{1+\exp((\phi_n-\phi_o)/k_BT)} \right|, \tag{2}$$

and ϕ_o is the intrinsic barrier height relative to E_f at $T=0$ K. Figure 4(a) shows that the conductance of the junction has only a slight dependence on temperature. There is no obvious impact on the shape of the $G(V)$, but the zero bias conductance (G_o) increases with temperature. Room temperature finds only a 6% increase in G_o, while it has increased by 30% for 600 K. As the temperature dependence of G_o is one of the Rowell criteria and is used to check for pinholes, we present the temperature dependence of G_o in Fig. 4(b); the resistance-area product of the junction ($1/G_o$) is often quoted rather than G_o, so its temperature dependence is shown for ease of comparison to literature.

Thermal smearing has a very minor impact on the conductance, which implies that the barrier parameters themselves must be relatively independent of temperature. As shown in Fig. 4(c), this is precisely what is found when we extract the effective barrier parameters (ϕ_{eff} and s_{eff}) by fitting G(V,T) with the BDR model; a barrier with $\phi_o=1$ eV and $s_o=15$ Å has deviations of ϕ_{eff} and s_{eff} from ϕ_o and s_o by less than 4% and 1%, respectively, for temperatures as high as 450 K. Thus, the same basic behavior seen in Sec. III A is reproduced for the height distribution associated with the Fermi–Dirac distribution, although with reduced impact; a distribution of barrier heights causes the net conductance to resemble that of a perfect barrier that is lower and wider than ϕ_o and s_o. At 450 K, for instance, the FWHM of $\alpha(\phi_n)$ is about 0.14 eV (14% of ϕ_o), yet the effective height decreases moderately to 0.97 eV. This is a small shift relative to the Gaussian results where a similar FWHM (σ) lead to ϕ_{eff} $\sim$0.77 eV [Fig. 2(a)]. The Fermi–Dirac height distribution has a less significant impact on the effective barrier parameters because it decays more rapidly than the Gaussian distribution [Fig. 4(d)].

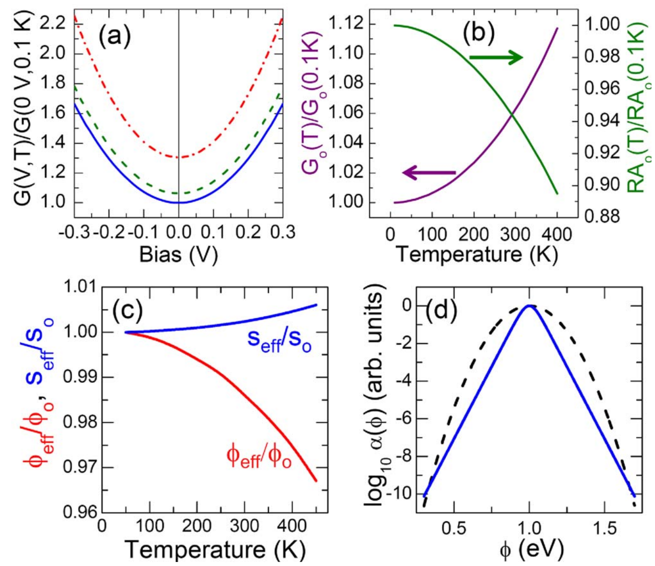

FIG. 4. (Color online) Thermal smearing simulations for junctions with $\phi_o=1$ eV and $s_o=15$ Å. (a) Bias dependence of tunneling conductance for 0.1 K (blue, solid), 300 K (green, dash), and 600 K (red, dash-dot). (b) The slight insulatorlike temperature dependence of the zero bias conductance (purple), and equivalently the resistance-area product (green), is a signature of tunneling, and is one of Rowell's tunneling criteria. (c) The best fit barrier thickness (blue) and height (red) change only slightly over a large temperature range, influenced only by thermal smearing. (d) The Fermi–Dirac barrier height distribution (solid) has a less pronounced impact on the effective barrier parameters than the Gaussian distribution (dash) because of its more rapid decay.

IV. DISCRETE TUNNELING CHANNELS

A. Secondary channels

This formalism is also amenable to modeling discrete, appropriately weighted, parallel tunneling channels. An example is the existence of a conduction channel with lower barrier height than the intrinsic barrier, which one might consider as an impurity of sorts. The secondary channel could represent, without loss of generality, areas where local strain has perturbed electronic structure, grain boundaries, or simply inhomogeneous phases within the electrodes or barrier. To this end, we modeled a junction with a secondary channel of variable weight whose height was half the primary height ($\phi_s=\phi_o/2$) and whose width was fixed at 20 Å. The weighting, ρ, represents without loss of generality, the relative area of the junction whose height is ϕ_s. We again assume a properly normalized distribution of weighting coefficients, $\alpha(\phi_n)/\Sigma_n\alpha(\phi_n)$, where

$$\alpha(\phi_n) = \begin{cases} 1, & \text{if } \phi_n=\phi_o, \\ \rho, & \text{if } \phi_n=\phi_s, \\ 0, & \text{otherwise}. \end{cases} \tag{3}$$

The net current density is calculated as above, and the resulting conductance is fit with the BDR model to extract the effective barrier parameters.

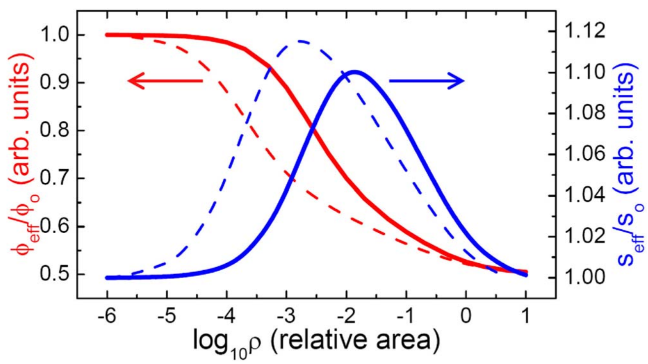

FIG. 5. (Color online) Best fit barrier height and width for the two-channel junction as a function of the relative weighting of the secondary channel. Solid: $\phi_o=1$ eV, $\phi_s=0.5$ eV; Dashed: $\phi_o=2$ eV, $\phi_s=1$ eV.

Figure 5 shows the impact of the secondary channel on the effective barrier parameters for two junctions, A with $\phi_o=1$ eV and $\phi_s=0.5$ eV (solid curves) and B with $\phi_o=2$ eV with $\phi_s=1$ eV (dashed curves). For junction A, the conductance is nearly independent of the second channel for densities less than 10 parts-per-million (ppm), whereas junction B is affected around the 1 ppm level. The influence of the secondary channel becomes severe by 1000 ppm for A, and 100 ppm for B. An in-depth analysis reveals that the secondary channel begins to dominate the conduction at the inflection point of the best fit barrier height curve. Figure 6 shows the relative density of the secondary channel required to contribute equally to the current density, ρ_{eq}, flowing through the junction for various primary barrier parameters. It can be seen that a secondary barrier height of 0.5 eV (for primary height of 1.0 eV) will support half of the current density if it represents 0.286% of the total junction area. This is, again, a hot spot. Further, ρ_{eq} decreases exponentially as either the barrier height or thickness increases. The latter implies that low, thin junctions are less susceptible to the impact of secondary tunneling channels. Putting this into context, a 20 Å MgO barrier with an expected 4 eV barrier height could have a net conductance indicative of bulk MgO only if secondary tunneling channels existed below the parts-per-billion level, and provided that those secondary heights exceed 1 eV. This seemingly improbable constraint could be a major reason that high barrier height junctions are rarely observed with transport measurements.[25]

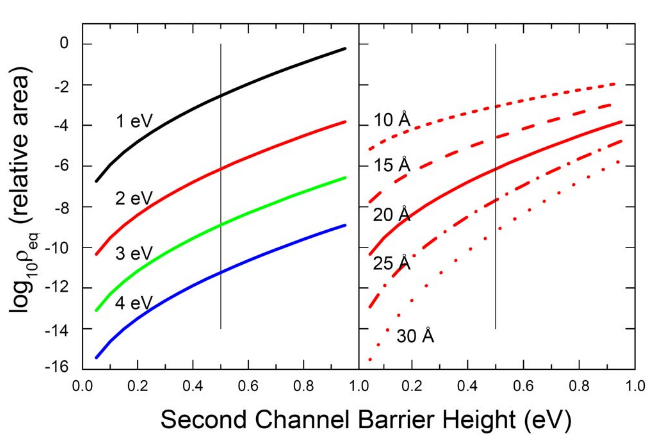

FIG. 6. (Color online) Relative impurity density required for primary and secondary tunneling channels to contribute equally to the net current density (ρ_{eq}) as a function of the secondary barrier height for the noted primary barrier heights with $s=20$ Å (left), and the noted thicknesses for a primary height of 2 eV. The thin vertical lines indicate 0.5 eV.

B. Spin filter tunneling

One particularly interesting concept that can be addressed with discrete tunneling channels is that of spin filter tunneling.[26–36] This phenomenon relies on a tunnel barrier material whose conduction band is spin split, which leads to different tunnel barrier heights for spin-up and spin-down electrons. As it is only the barrier that dictates the net tunneling spin polarization, the most unique attribute of spin filter tunneling is its ability to generate spin polarized currents using entirely nonmagnetic electrodes.

There are two parallel channels in spin filter junctions, one for each spin. Spin-up and spin-down electrons see different barrier heights below the ordering temperature of the magnetic insulator. The spin channel with the lower barrier height has a larger transmission coefficient, which implies that the current entering the collector electrode is spin polarized. This polarization is typically expressed as $P=(j_\uparrow-j_\downarrow)/(j_\uparrow+j_\downarrow)$, where the spin-dependent current densities are calculated using spin and temperature dependent barrier heights. The individual tunneling current densities are calculated as above, with the net current density being their average $j_{\text{net}}=(j_\uparrow+j_\downarrow)/2$. Assuming that the exchange splitting is proportional to the magnetization allows us to define the temperature dependence of the two barrier heights above and below the magnetic ordering temperature, T_c,

$$T \le T_c: \begin{cases} \phi_\uparrow = \phi_o - \Delta E_{\text{ex}}\sqrt{1-T/T_c} \\ \phi_\downarrow = \phi_o + \Delta E_{\text{ex}}\sqrt{1-T/T_c} \end{cases}$$

$$T > T_c: \phi_\uparrow = \phi_\downarrow = \phi_o. \tag{4}$$

The net current density and net conductance are calculated as above, allowing the experimentally observed temperature dependence to be reproduced. As the temperature falls below T_c, the zero-bias resistance-area product (i.e., $1/G_o$) drops dramatically, while the spin polarization expeditiously increases (Fig. 7). This is the direct result of $\phi_\uparrow$ and $\phi_\downarrow$ separating below T_c.

V. CONCLUSIONS

In summary, we have shown that implementing continuous and discrete tunnel barrier heights distributions enables straightforward modeling of multiple phenomena of importance to tunneling. For continuous tunneling channels, a random distribution of heights causes ideal tunneling models to find faulty barrier parameters, with the incurred errors strongly dependent on the variance. The temperature dependence associated with tunneling was demonstrated by transferring the thermal smearing of the electrodes to the barrier potential energy; zero-temperature tunneling models are thereby given the ability to model temperature dependent tunneling. For discrete tunneling channels, we showed that a secondary channel can dominate the net conductance at surprisingly low impurity levels, making the observation of in-

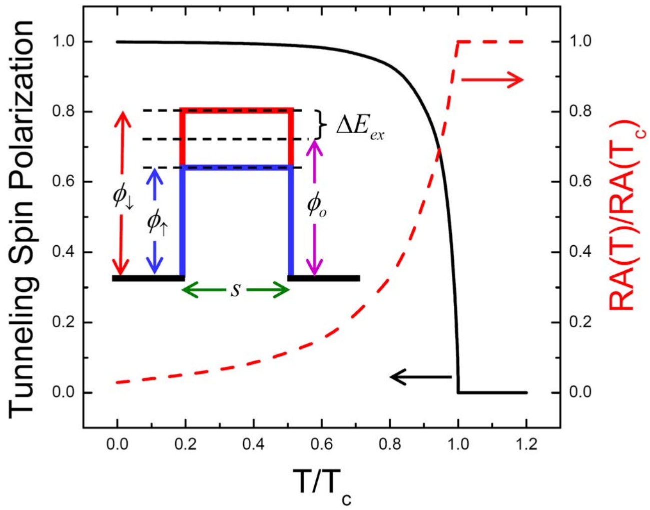

FIG. 7. (Color online) The normalized resistance-area product (RA) at zero bias (red, dashed) decreases as the spin-polarization (p) of tunneling electrons (black, solid) increases when the temperature falls below T_c. The parameters used were $\phi_o = 1$ eV, $2\Delta E_{ex} = 0.5$ eV, and $s = 30$ Å. (Inset) Illustration of spin filter tunneling barrier parameters below T_c, according to Eq. (4).

trinsically large barrier heights highly unlikely with transport measurements. This concept was then applied to spin-dependent tunneling channels, allowing the temperature dependence of a spin-filter barrier to be reproduced.

ACKNOWLEDGMENTS

Supported by the National Science Foundation, the Center for Integrated Functional Materials is supported by the USAMRMC.

[1] W. F. Brinkman, R. C. Dynes, and J. M. Rowell, J. Appl. Phys. **41**, 1915 (1970).
[2] J. G. Simmons, J. Appl. Phys. **34**, 1793 (1963).
[3] C. W. Miller, Z.-P. Li, J. Åkerman, and I. K. Schuller, Appl. Phys. Lett. **90**, 043513 (2007).
[4] J. D. R. Buchanan, T. P. A. Hase, B. K. Tanner, N. D. Hughes, and R. J. Hicken, Appl. Phys. Lett. **81**, 751 (2002).
[5] C. Tusche, H. L. Meyerheim, N. Jedrecy, G. Renaud, A. Ernst, J. Henk, P. Bruno, and J. Kirschner, Phys. Rev. Lett. **95**, 176101 (2005).
[6] C. W. Miller, Z.-P. Li, I. K. Schuller, R. W. Dave, J. M. Slaughter, and J. Åkerman, Phys. Rev. B **74**, 212404 (2006).
[7] R. K. Singh, R. Gandikota, J. Kim, N. Newman, and J. M. Rowell, Appl. Phys. Lett. **89**, 042512 (2006).
[8] W. H. Rippard, A. C. Perrella, and R. A. Buhrman, Appl. Phys. Lett. **78**, 1601 (2001).
[9] O. Kurnosikov, J. E. A. de Jong, H. J. M. Swagten, and W. J. M. de Jonge, Appl. Phys. Lett. **80**, 1076 (2002).
[10] P. G. Mather, J. C. Read, and R. A. Buhrman, Phys. Rev. B **73**, 205412 (2006).
[11] P. H. P. Koller, H. J. M. Swagten, W. J. M. de Jonge, H. Boeve, and R. Coehoorn, Appl. Phys. Lett. **84**, 4929 (2004).
[12] L. S. Dorneles, D. M. Schaefer, M. Carara, and L. F. Schelp, Appl. Phys. Lett. **82**, 2832 (2003).
[13] T. S. Yoon, T. Shoyama, Y. W. Lee, M. Tsunoda, M. Takahashi, D. Y. Kim, and C. O. Kim, J. Magn. Magn. Mater. **284**, 330 (2004).
[14] Y. Ando, H. Kameda, H. Kubota, and T. Miyazaki, J. Appl. Phys. **87**, 5206 (2000).
[15] I. Giaever, Phys. Rev. Lett. **5**, 147 (1960).
[16] J. M. Rowell, in *Tunneling Phenomena in Solids*, edited by E. Burnstein and S. Lundqvuist (Plenum Press, New York, 1969), pp. 385–404.
[17] J. J. Åkerman, I. V. Roshchin, J. Slaughter, R. W. Dave, and I. K. Schuller, Europhys. Lett. **63**, 104 (2003).
[18] C. W. Miller, I. K. Schuller, R. W. Dave, J. M. Slaughter, Y. Zhou, and J. Åkerman, J. Appl. Phys. **103**, 07A904 (2008).
[19] C. W. Miller, Z.-P. Li, I. K. Schuller, R. W. Dave, J. M. Slaughter, and J. Åkerman, Phys. Rev. Lett. **99**, 047206 (2007).
[20] C. H. Shang, J. Nowak, R. Jansen, and J. S. Moodera, Phys. Rev. B **58**, R2917 (1998).
[21] J. J. Åkerman, J. M. Slaughter, R. W. Dave, and I. K. Schuller, Appl. Phys. Lett. **79**, 3104 (2001).
[22] J. J. Åkerman, R. Escudero, C. Leighton, S. Kim, D. A. Rabson, R. W. Dave, J. M. Slaughter, and I. K. Schuller, J. Magn. Magn. Mater. **240**, 86 (2002).
[23] D. A. Rabson, B. J. Jönsson-Åkerman, A. H. Romero, R. Escudero, C. Leighton, S. Kim, and I. K. Schuller, J. Appl. Phys. **89**, 2786 (2001).
[24] B. J. Jönsson-Åkerman, R. Escudero, C. Leighton, S. Kim, I. K. Schuller, and D. A. Rabson, Appl. Phys. Lett. **77**, 1870 (2000).
[25] W. H. Butler, X.-G. Zhang, S. Vutukuri, M. Chshiev, and T. C. Schulthess, IEEE Trans. Magn. **41**, 2645 (2005).
[26] J. S. Moodera, T. S. Santos, and T. Nagahama, J. Phys.: Condens. Matter **19**, 165202 (2007).
[27] T. S. Santos, J. S. Moodera, K. V. Raman, E. Negusse, J. Holroyd, J. Dvorak, M. Liberati, Y. U. Idzerda, and E. Arenholz, Phys. Rev. Lett. **101**, 147201 (2008).
[28] X. Hao, J. S. Moodera, and R. Meservey, Phys. Rev. B **42**, 8235 (1990).
[29] J. S. Moodera, R. Meservey, and X. Hao, Phys. Rev. Lett. **70**, 853 (1993).
[30] T. S. Santos and J. S. Moodera, Phys. Rev. B **69**, 241203 (2004).
[31] M. Gajek, M. Bibes, A. Barthélémy, K. Bouzehouane, S. Fusil, M. Varela, J. Fontcuberta, and A. Fert, Phys. Rev. B **72**, 020406 (2005).
[32] M. Gajek, M. Bibes, M. Varela, J. Fontcuberta, G. Herranz, S. Fusil, K. Bouzehouane, A. Barthélémy, and A. Fert, J. Appl. Phys. **99**, 08E504 (2006).
[33] U. Lüders, M. Bibes, K. Bouzehouane, E. Jacquet, J.-P. Contour, S. Fusil, J.-F. Bobo, J. Fontcuberta, A. Barthélémy, and A. Fert, Appl. Phys. Lett. **88**, 082505 (2006).
[34] A. V. Ramos, M.-J. Guittet, J.-B. Moussy, R. Mattana, C. Deranlot, F. Petroff, and C. Gatel, Appl. Phys. Lett. **91**, 122107 (2007).
[35] G.-X. Miao and J. S. Moodera, Phys. Rev. Lett. **102**, 076601 (2009).
[36] C. W. Miller, J. Magn. Magn. Mater. (in press).